Enabling High-Temperature Superconducting Magnets on Small Satellites Using a Miniature Cryocooler

J. R. Olatunji, N. M. Strickland, T. Berry, E. V. W. Chambers, S. C. Wimbush

Paihau-Robinson Research Institute, Victoria University of Wellington, Wellington, New Zealand

ABSTRACT

High-temperature superconducting (HTS) tapes can carry very large electrical currents through very thin wires with no electrical resistance. This means HTS tape can be wound into lightweight, high field electromagnets that do not generate heat. HTS electromagnets therefore have the potential to be very useful in the space domain, which has extreme size and weight restrictions, and where it can be difficult to radiatively dissipate the amount of heat generated by conventional copper electromagnets. HTS is therefore posited as a miniaturisation technology capable of generating high magnetic fields onboard small satellites for applications such as electric propulsion, radiation shielding, attitude control, and inductive energy storage.

HTS devices require to be operated at cryogenic temperatures, typically at or below 77 K. Maintaining these cryogenic temperatures in space can be achieved using an electrical cryocooler. The nature of the cryocooler and how it is integrated with the HTS electromagnet has a significant impact on the SWaP (size, weight and power) requirements.

This paper presents modelling and preliminary physical testing of an HTS electromagnet design intended to be integrated into a CubeSat. This work investigated whether a single miniature cryocooler can cool an HTS electromagnet to below its critical temperature, using a combined numerical modelling and experimental approach. Using a Sunpower CryoTel MT cryocooler, weighing only 2.1 kg and with a length and diameter of just 243 mm and 73 mm, respectively, an electromagnet temperature of less than 75 K was obtained using only 40 W of input power while maintaining a 40 °C hot end temperature. This suggests that HTS electromagnets can be operated on board small satellites using miniature, single stage cryocoolers.

INTRODUCTION

Recent advances in miniature cryocoolers have reinvigorated the discussion of using high-temperature superconductors (HTS) for space applications. HTS tapes have very favorable properties for the space industry, as the combination of large current densities and zero electrical resistance means the creation of lightweight, high field electromagnets that do not generate heat while operating. Superconductivity as a phenomenon appears at cryogenic temperatures, hence the need for an active cooling system such as a cryocooler.

The useful applications of HTS electromagnets for space are potentially numerous and have been discussed elsewhere [1]. Of particular interest to Paihau-Robinson Research Institute are the enhancement of electric thrusters with HTS electromagnets, such as applied-field magnetoplasmadynamic (AF-MPD)

Cryocoolers 22, edited by R.G. Ross, Jr., J.R. Raab and S.D. Miller

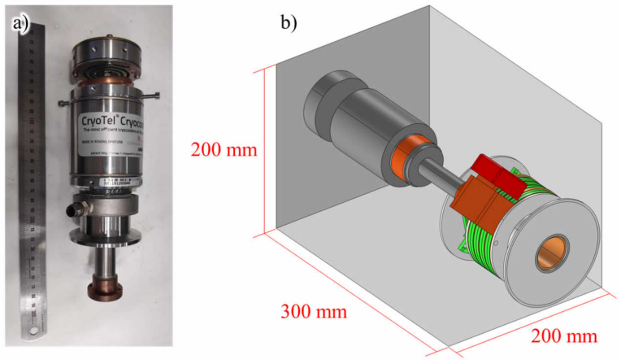

Figure 1. a) A Sunpower CryoTel MT Cryocooler. b) Concept drawing showing an HTS-AF-MPD thruster and Sunpower CryoTel MT cryocooler fitting within the volume of a 12U CubeSat.

thrusters. AF-MPD thrusters use electric and applied magnetic fields to accelerate plasma to velocities an order of magnitude greater than chemical thrusters. It has been shown that stronger applied magnetic fields increase thrust, power specific thrust, and efficiency [2-5].

Positing HTS as a miniaturisation technology, Paihau-Robinson Research Institute are developing an HTS-AF-MPD thruster for a small satellite. The combination of a miniature cryocooler and small HTS electromagnet could potentially create a thruster with a very favourable SWaP (size weight and power) profile. This, however, represents a significant thermal and power management problem. Although devices based on HTS thin films have been successfully operated in space [6], there are no public reports of space operating HTS electromagnets. The most common use for cryocoolers on satellites in low-Earth orbit (LEO) is infrared spectroscopy [7], for which the thermal management of HTS devices is much more complex. HTS electromagnets must be cooled to below ~77 K for useful magnetic field strengths to be generated, whereas infrared cameras require ~110 K. Secondly, HTS electromagnets are much larger and more massive than device chips on infrared cameras, making cooling demands and the cryogenic design more complex.

We showed previously that fields up to 1T can be generated with an HTS electromagnet on a 3U CubeSat [8]. However, this study was entirely hypothetical, did not consider a particular cryocooler, and had a magnet design unsuitable for use with a thruster. Therefore, in this paper, we present experimental and modelling results for the thermal testing of an HTS electromagnet and cryocooler combination, to provide evidence that small cryocoolers are a key enabling technology for the use of HTS in space on small satellites, and that the power and thermal management problems are not insurmountable. As we were uncertain of the cryocooler performance demands of such an HTS electromagnet, at this stage we opted to perform testing on a 'replica magnet' with similar mass, size and thermal properties, so that we can validate our design assumptions before manufacturing real HTS coils.

After a search of commercial miniature space rated cryocoolers, the Sunpower CryoTel MT cryocooler (Figure 1a) was chosen as the most appropriate for our project goals [9]. This cryocooler was advertised as a 5 W cryocooler at 77 K, weighing 2.1 kg and having a length and diameter of 243 mm and 73 mm, respectively. This makes it appropriate for use on a range of CubeSats, such as 3U, 6U or 12U (Figure 1b).

MATERIALS AND METHODS

Cryocooler Performance

The performance of the Sunpower CryoTel MT cryocooler was measured across a range of input powers and hot-end temperatures (Figure 2a). The performance of the cryocooler was linearly dependent on the Carnot efficiency and the input power, so that a simple empirical performance formula could be generated:

$$Q_c = a \cdot \epsilon_c + b \begin{cases} a = 0.2917 \cdot P_{in} + 2.7483 \\ b = -0.0213 \cdot P_{in} - 2.5443 \end{cases} \quad (1)$$

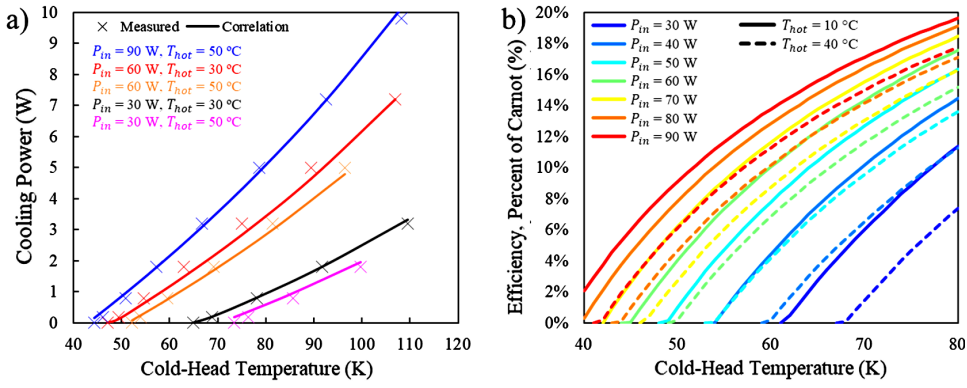

Figure 2. a) Measured performance curves at different combinations of input power and hot-end temperature. Crosses are data points and lines are the result of applying equations (1) and (2); b) efficiency of the cryocooler across different operating conditions.

where Q_c is the cooling power generated at the cold-end (W), P_{in} is the input power (W), a and b are curve-fitted coefficients, and ϵ_c is the Carnot efficiency:

$$\epsilon_c = T_{cold}/(T_{hot} - T_{cold}) \tag{2}$$

where T_{cold} and T_{hot} are the cold and hot-end temperatures of the cryocooler (K). The performance of Eq. (1) is shown in Figure 2a, and had a mean average error of just ±0.15 W. The efficiency of this cryocooler is shown across the entire operability range in Figure 2.

HTS Electromagnet Design

The preliminary design for this HTS electromagnet required a bore large enough to fit a reasonably sized cylindrical anode for the thruster, and sufficient clearance for vacuum suspension with many layers of multilayer insulation (MLI) to thermally isolate the magnet, resulting in Figure 3.

Using 4 mm wide REBCO HTS tape, this design consisted of four double-pancake (DP) coils with an inner diameter (ID) of 64 mm and outer diameter (OD) of 90 mm, epoxy impregnated into 7.5 mm wide G10 rings. In between DPs were 1 mm thick copper cooling plates, and the entire assembly was mechanically secured between stainless steel plates using 5 mm diameter stainless steel pins. The copper cooling plates were bolted to a copper thermal bus, which in turn was mounted to the cold-head of a cryocooler.

Energising the HTS electromagnet with copper wires was shown to be unfeasible for space applications in our previous work [8], representing over 97% of the total heat leak. Therefore, a superconducting flux pump [10] is used to energise the electromagnet. Precise details of the operability of the flux pump are

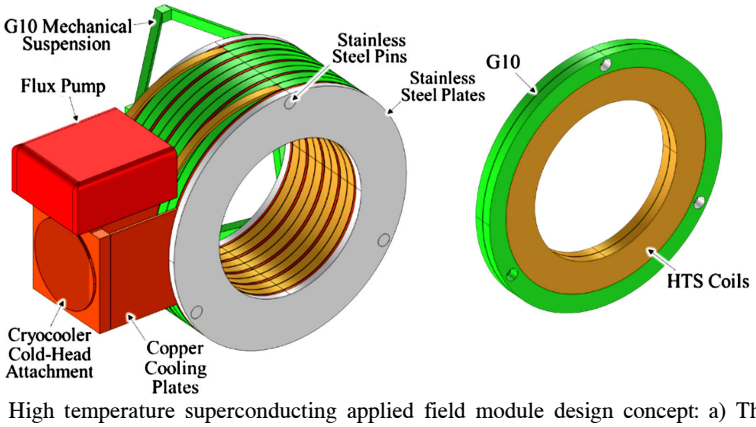

Figure 3. High temperature superconducting applied field module design concept: a) The entire flight magnet assembly including mechanical and structural supports, thermal bus and energisation source; b) An individual double-pancake HTS coil.

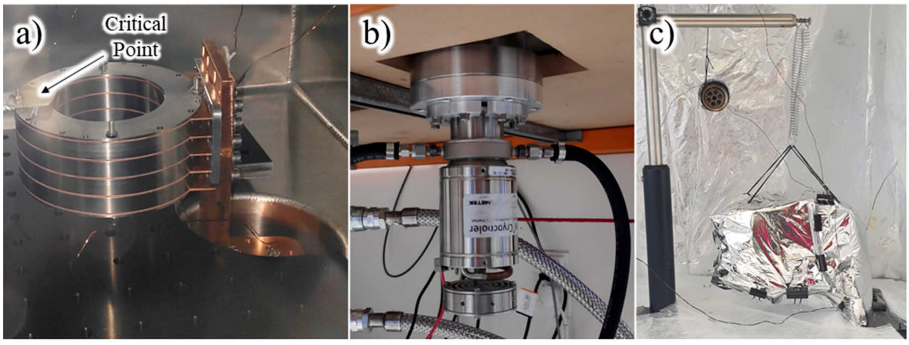

Figure 4. a) Replica magnet assembled on the cryocooler inside a vacuum chamber; b) the Sunpower CryoTel MT cryocooler installed through a port on the vacuum chamber; c) the replica magnet and vacuum chamber walls insulated against radiation using multilayer insulation.

omitted in this paper, but as it is also a superconducting component, it must also be kept at cryogenic temperatures, and so is also attached to the copper thermal bus.

The magnet assembly was mechanically vacuum suspended using 2.5 mm thick G10 struts. G10 is mechanically strong with a low thermal conductivity.

We aim to demonstrate in this paper that this cryogen-free design can conductively cool the magnet to cryogenic temperatures with favourable SWaP characteristics: there is room for a 50 mm diameter anode in the bore of the magnet; this assembly could fit into a 6U or 12U CubeSat; and the magnet assembly weighs only 1.5 kg (plus a 2.2 kg cryocooler).

Experimental Set-Up

A replica magnet was designed to have a similar thermal mass and thermal properties to the HTS magnet described in Figure 3. This consisted of stainless-steel disks with the same height, ID and OD of a double-pancake HTS coil (Figure 4a).

PT-100 temperature sensors were mounted to the magnet critical point, thermal bus, and cryocooler cold-head. The magnet critical point is defined as the position with the lowest critical current (worst performance) during operation. If this point is held below our target temperature, then we are confident the critical current in the rest of the magnet is above the operating current.

Thermal testing was performed within a vacuum chamber. Thermal grease was applied to mating surfaces and all connections were bolted tight to improve the thermal conduction at joins.

The effect of wrapping the replica electromagnet in MLI to shield it from incident thermal radiation from the room-temperature surroundings was investigated, first testing the magnet without MLI, then 10 layers, 20 layers, and finally 30 layers (20 on the magnet and 10 on the chamber walls). The final experimental setup showing the magnet within the vacuum chamber mounted to the cryocooler (with 30 layers of MLI) is shown in Figure 4c.

The cryocooler was operated at its maximum rated input power of 90 W. Availability of this level of continuous power on a small satellite is likely not viable, and so was also operated at a more feasible 40 W. Tests were conducted using a hot-end temperature of 20 °C, using water cooling. Tests were also performed to investigate the effects of changing the hot-end temperature in the range 20–40 °C.

Model Formulation

A 3D finite element model was formulated in COMSOL v6.0. Fourier's law was solved to predict temperature change:

$$\rho C_p(T)\frac{\partial T}{\partial t} = \nabla \cdot (\lambda(T)\nabla T + Q_{rad}) + Q \tag{3}$$

where ρ is the density (kg·m^{-3}), $C_p(T)$ is the temperature dependent specific heat capacity (J·kg^{-1}·K^{-1}), $\lambda(T)$ is the temperature dependent thermal conductivity (W·m^{-1}·K^{-1}), T is the temperature (K), t is time (s), Q_{rad} is radiative heat flux (W·m^{-2}), and Q are any additional custom heat sources (W·m^{-3}). Temperature

Table 1. Temperature dependent thermal properties [11]. T: temperature; λ: thermal conductivity; C_p: specific heat capacity; h: thermal contact conductivity.

	HTS composite		Copper			Aluminium		Stainless steel		G10	
T	λ	C_p	h	λ	C_p	λ	C_p	λ	C_p	λ	C_p
K	W/m·K	J/kg·K	W/m²·K	W/m·K	J/kg·K	W/m·K	J/kg·K	W/m·K	J/kg·K	W/m·K	J/kg·K
4	0.3	1.1	110.8	126.0	0.1	3.3	0.3	0.3	2.0	0.07	2.0
10	0.7	3.4	271.5	313.3	0.9	8.4	1.4	0.9	5.2	0.11	15.4
20	1.2	13.5	504.7	593.4	7.9	17.0	8.9	2.2	17.0	0.16	47.0
40	1.8	51.5	757.9	731.6	55.6	33.0	87.0	4.7	55.0	0.22	115.0
77	2.4	194.9	991.5	442.6	187.1	55.0	336.0	7.9	200.0	0.28	239.0
100	2.6	253.0	1073.0	394.1	253.0	66.0	481.0	9.2	250.0	0.31	317.0
150	3.2	344.8	1176.9	380.0	331.7	85.0	684.0	11.2	350.0	0.37	489.0
200	3.7	388.6	1221.6	383.7	362.0	99.0	797.0	12.6	400.0	0.44	664.0
300	5.1	444.4	1266.3	384.0	377.0	118.0	902.0	15.3	480.0	0.61	999.0

dependent thermal properties were derived from a literature source [11], presented in Table 1. These were imported into COMSOL as interpolation tables for each material.

Four models were developed, summarised in Figure 5.

The first model (Figure 5a) was the replica magnet for which thermal testing was performed. The cryocooler was applied through a negative heat source at the surface of the cold-head, $Q_c(T_{cold}, T_{hot}, P_{in})$ (W). Q_c is defined by Eq. (1), T_{hot} and P_{in} are model inputs, and T_{cold} is probed as the average temperature of this surface. All surfaces were in radiative thermal exchange with the ambient environment using COMSOL's

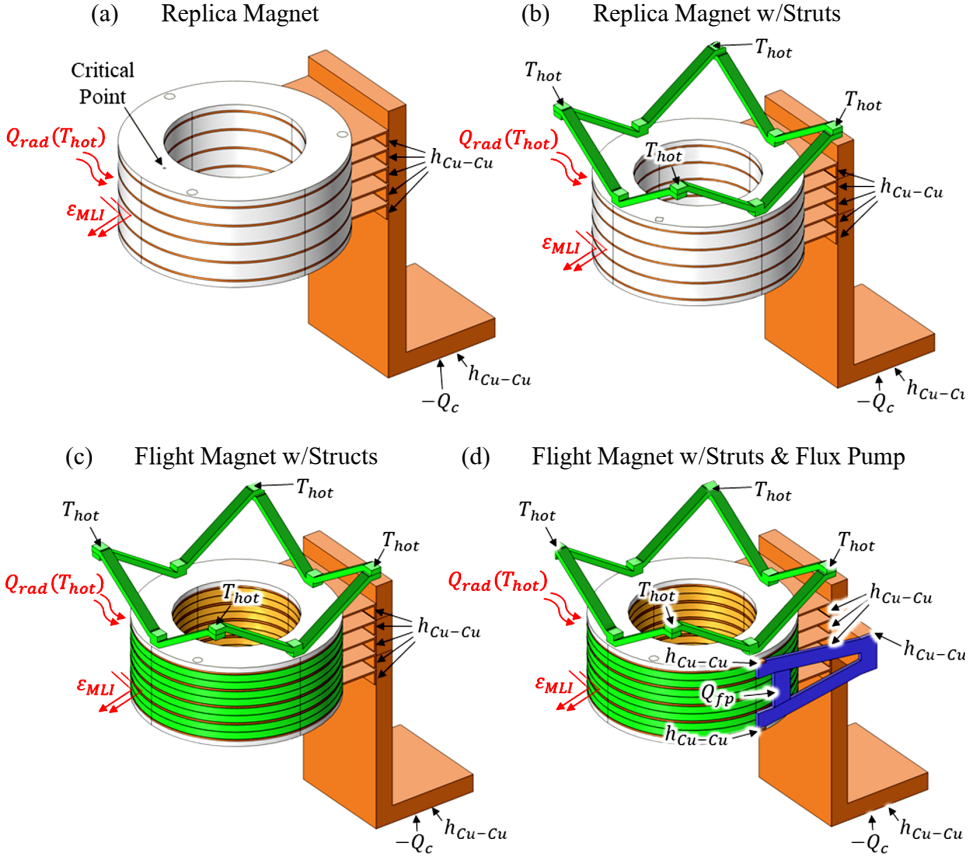

Figure 5. Model geometries, boundary conditions and material selection: a) replica magnet; b) replica magnet with struts; c) flight magnet with struts; d) flight magnet with struts and flux pump.

'surface-to-surface radiation' module, for which the ambient temperature, T_{amb} (K), and the effective emissivity of the MLI wrapped magnet, ε_{MLI}, were vital inputs. Assuming the cryocooler is in good thermal contact with the satellite, $T_{amb} = T_{hot}$. At joining copper surfaces a temperature dependent thermal contact conductivity, $h_{Cu\text{-}Cu}(T)$ ($W \cdot m^{-2} \cdot K^{-1}$), was applied. This was taken from [11] as Cu-Cu joins with 50 kg of force applied (see Table 1).

By tuning and validating this first model, we can propagate the validated model forward and inspect the impact of adding space-necessary features on thermal performance. Our second model added G10 mechanical suspension to the replica magnet (Figure 5b). The ends of the struts, being attached to the satellite, were set to a constant temperature of T_{hot}.

Our third model replaced the stainless-steel replica magnet with HTS coils, as described in Figure 3. The differences between the second and third model should be negligible if our replica magnet is representative of the thermal performance of a flight magnet.

Our fourth and final model added 2 mm thick aluminum structures to represent a flux pump, which is used to energise our coils. Our flux pump is a superconducting device that will generate heat while operating, so a domain heat source, Q_{fp}, is defined at the middle section.

RESULTS AND DISCUSSION

Experimental Results

Thermal testing with a hot-end temperature of 20 °C is summarised in Figure 6. It was found that the magnet critical point reached the target temperature of below 77 K when wrapped in 10 MLI layers for 90 W input power, and but only required 40 W with 30 MLI layers.

The experiments were repeated at different hot-end temperatures. As expected, the efficiency of the cryocooler declined at higher hot-end temperatures, aligning closely with the loss of Carnot efficiency. As the hot-end temperature is closely linked to the satellite body temperature, the temperature-dependent performance of the cryocooler is necessary to model. This is shown later (Figure 7 and Figure 10).

Overall, the number of MLI layers used had a profound impact on the temperature of the magnet. This reflects the fact that the radiation heat load is expected to be the largest contributor, in the absence of a magnet power supply.

These results were encouraging, as they suggest that with appropriate wrapping, we can achieve our target temperature with cryocooler input powers well below the 90 W limit for our chosen cryocooler.

Model Validation

The model was tuned and validated through several comparisons to measurement. There were important model unknowns, such as the effective emissivity of the MLI, ε_{MLI}, and the thermal contact conductivity of Cu-Cu joints, $h_{Cu\text{-}Cu}$. The following used measurements taken with 30 MLI layers.

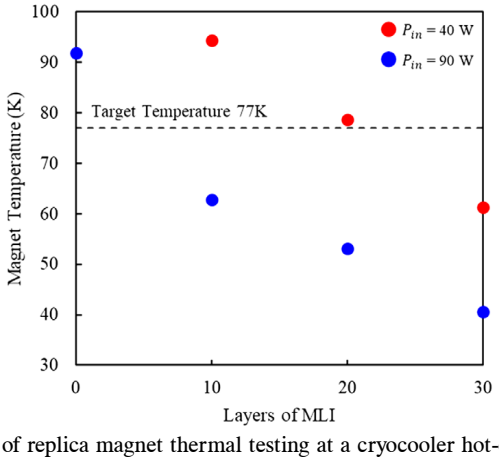

Figure 6. Summary of replica magnet thermal testing at a cryocooler hot-end temperature of 20 °C, for different layers of wrapping and different cryocooler input powers.

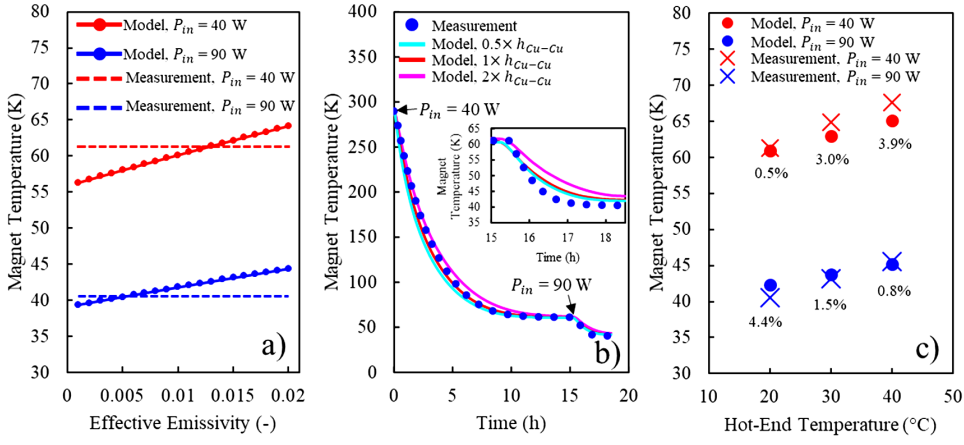

Figure 7. Model validation and tuning: a) steady-state temperature of the replica magnet at different effective emissivities of the MLI wrapping; b) transient temperature of the replica magnet at different Cu-Cu contact conductivities (inset) close up of the increase from 40 to 90 W input power; c) steady-state temperature of the replica magnet at different cryocooler hot-end temperatures, numbers signifying the percentage difference between model and measurements.

First, grid independence was confirmed by running steady state simulations at two mesh sizes (9354 and 42598 elements). Using P_{in} = 40 W, ε_{MLI} = 0.01, T_{hot} = 20 °C and $h_{Cu\text{-}Cu}$ as stated in Table 1, the difference in the critical point temperature was less than 0.1%. We therefore chose to use the coarser mesh for the remaining work.

Second, the effective emissivity was derived by running a series of steady-state simulations with different ε_{MLI} values. Shown in Figure 7a, it was observed that the emissivity appears to be temperature dependent, being lower at colder temperatures. However, ε_{MLI} = 0.012 gives the smallest total error; therefore this is propagated through the remainder of this work as being representative of 30 MLI layers.

Third, the contact conductivity of Cu-Cu joins was determined by performing transient simulations. Shown in Figure 7b the cryocooler input power was initially set to 40 W, and then increased to 90 W at 15.35 h. The temperature dependent contact conductivity of Cu-Cu joins was scaled from 0.5 to 2 times the values shown in Table 1. This showed that no re-scaling was necessary, and the values from [11] are appropriate for modelling cryogenic Cu-Cu joins.

Our model slightly over predicted the cooling rate at the beginning of the cooling process, but equilibrated to 60.9 K, less than 1 K from the measurement. Increasing input power to 90 W, our model slightly under predicted the cooling rate, but again equilibrated to within 2 K of the measurement.

Finally, the model was compared to measurements where the cryocooler hot-end temperature was increased (Figure 7c). Our model showed good agreement, matching with the decline in cryocooler efficiency at higher hot-end temperatures.

In totality, this validates our thermal model in several important ways: it shows that using temperature dependent thermal properties from literature sources is appropriate; using literature derived thermal contact conductivities is also appropriate; our model can accurately predict the steady-state and time dependent temperature of our magnet; and that our cryocooler efficiency equation can be used to accurately predict the magnet temperature across any input power or hot-end temperature. We can therefore use this model to accurately predict the thermal behavior of our magnet and cryocooler combination to within 5% over any conditions.

Model Application

Having validated the replica magnet model against experimental results, we explored the impact of adding space-necessary structures and components. Visualisations of our four models are shown in Figure 8, where P_{in} = 40 W and T_{hot} = 40 °C are used. We report the temperature at the magnet critical point, maximum and minimum temperature in Figure 9a; and the magnitude of different sources of heat leak in Figure 9b.

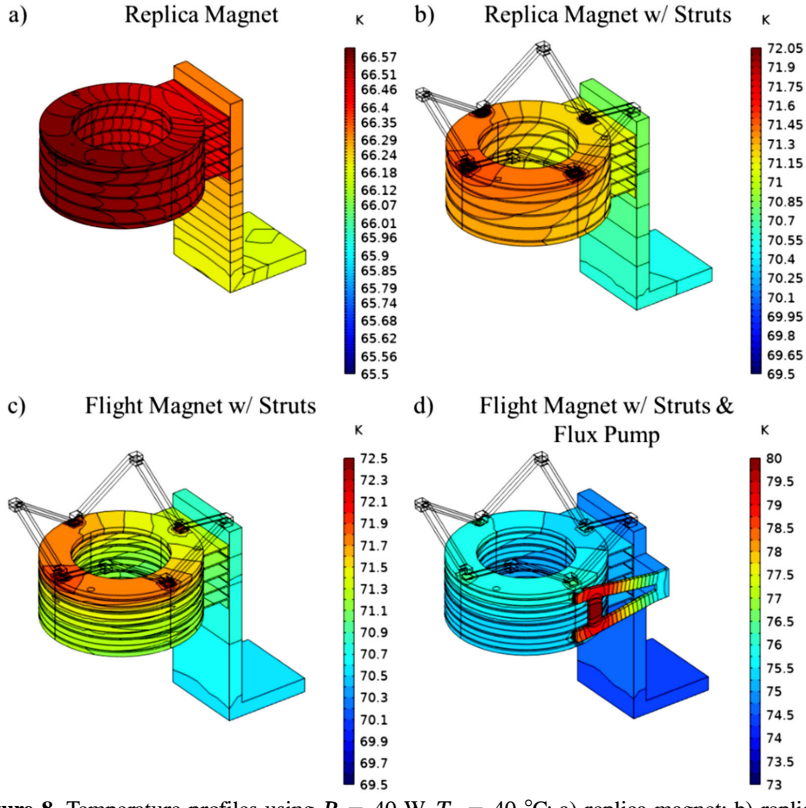

Figure 8. Temperature profiles using P_{in} = 40 W, T_{hot} = 40 °C: a) replica magnet; b) replica magnet with struts; c) flight magnet with struts; d) flight magnet with struts and a flux pump.

Our assumption that the critical point is representative of the maximum temperature is validated, as there is a negligible difference between these two temperatures. Adding struts adds Q_λ = 260 mW of conductive heat leak, increasing the magnet temperature by 4.9 K and increasing the temperature gradient from 0.1 K to 0.5 K. The differences between the replica and flight magnet were slight: only a 0.3 K

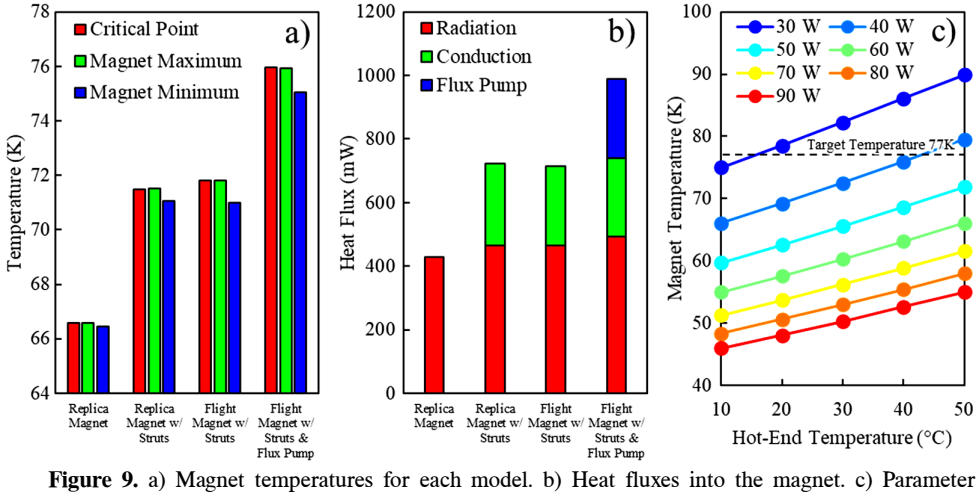

Figure 9. a) Magnet temperatures for each model. b) Heat fluxes into the magnet. c) Parameter sweep of the magnet temperature at different input powers and hot-end temperatures.

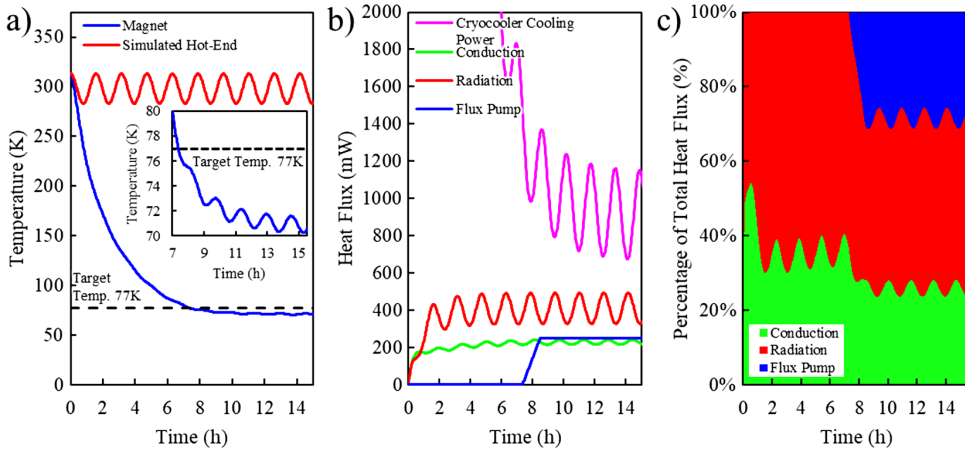

Figure 10. On-orbit cool-down time estimation: a) magnet and simulated hot-end temperatures (inset) close up of magnet temperature as it reaches the target temperature; b) heat fluxes; c) relative heat fluxes into cryogenic environment.

increase in temperature, but the flight magnet had a less uniform temperature profile. This is to be expected, as the addition of the G10 rings at the OD of the HTS coils represents a larger fraction of highly insulating material, slightly hindering the extraction of heat. Finally, for the flight magnet with a flux pump, we applied an additional Q_{fp} = 250 mW, which is a best estimate for the thermal performance of such a device. This raised the temperature by another 4 K and increased the temperature gradient to nearly 1 K. Even with the addition of all the necessary flight components, the magnet temperature was still under the 77 K target temperature.

We then used the model of the flight magnet with struts and a flux pump to sweep the parameter space, exploring input powers between 30-90 W and hot-end temperatures between 10-50°C. Shown in Figure 9c, the HTS magnet can be kept under the target 77 K for nearly all hot-end temperatures if the input power is greater than 40 W.

This is very encouraging as it suggests we can operate the Sunpower CryoTel MT cryocooler well below the maximum input power of 90 W, leaving a wide margin to account for errors in our model validation, and potentially to absorb even more sources of heat, such as the heat generated by the thruster while operating.

Finally, we used the model to simulate a transient magnet cooldown in space while on board a hypothetical satellite. Using Keplerian orbital mechanics, a perfectly circular 500 km altitude orbit was calculated to have an orbital period of 1.57 hours. Assuming the satellite spends half the orbit in direct solar radiation and half in the shadow of the Earth, we can approximate the temperature of the satellite to oscillate between a minimum and maximum temperature every orbit. If the cryocooler is sufficiently thermally anchored to the satellite, we can therefore approximate the hot-end temperature as a sine wave, oscillating between 10°C and 40°C every 1.57 hours. These are reasonable temperatures considering the large amount of radiation in a low-Earth orbit. The flux pump does not energise the magnet until it is at the target temperature. Therefore, Q_{fp} = 0 W if the magnet temperature is above 77 K, and 250 mW when below. Based on our findings in Figure 9c, we set P_{in} = 40 W and performed a transient simulation over 10 orbits.

Shown in Figure 10b, the magnet cool-down time was 7.4 h, with the final temperature oscillating between 70 and 72 K. This is due to changes in the cryocooler efficiency caused by oscillations of the hot-end temperature, as well as an oscillating heat load into the cryogenic environment from conduction and radiation, which are also a function of the satellite temperature. Radiative heat transfer had the largest variability due to $Q_{rad} \propto \Delta T^4$. Conduction was $Q_{\lambda} \propto \Delta T$, so had less of an impact. This oscillation could be prevented by implementing a control loop that altered the input power to the cryocooler as a function of the magnet temperature.

This result is, again, encouraging, as it suggests that only 40 W of cooling power is required to achieve the required cryogenic temperatures for superconductivity on a small spacecraft in orbit. 40 W of continuous input power is a large but not unfeasible level of power generation for mid-size CubeSats with deployable solar panels.

CONCLUSIONS

We have shown computationally that HTS electromagnets cooled by miniature single-stage cryocoolers are feasible for the generation of high magnetic fields on small spacecraft down to the CubeSat size, and we support our findings with experimental measurements of a replica magnet cooled by a Sunpower CryoTel MT cryocooler. These demonstrated that magnet operating temperatures below 75 K could be maintained, using only 40 W of input power while maintaining a 40°C cryocooler hot end temperature. The unaddressed challenges remaining for in-space operation include provision of sufficient power to operate the cryocooler for the extended times required, as well as dissipation of the waste heat generated by the cryocooler operation.

ACKNOWLEDGMENT

This work was funded by the New Zealand Ministry of Business, Innovation and Employment (project title: 'High Magnetic Field Electric Propulsion for Space', contract number RTVU2003).

REFERENCES

1. G. W. Mitschang, "Space applications and implications of high temperature superconductivity," *IEEE Transactions on Applied Superconductivity,* vol. 5, no. 2 (1995), pp. 69-73.
2. J. R. Olatunji, N. M. Strickland, M. R. G. Winchester, K. Kinefuchi, D. Ichihara, N. J. Long, and S. C. Wimbush, "Modelling of a 1 T High-Temperature Superconducting Applied Field Module for a Magnetoplasmadynamic Thruster," in *TENCON 2021-2021 IEEE Region 10 Conference (TENCON)* (2021), pp. 173-178.
3. H. Kasuga, J. Jeong, K. Mizutani, A. Iwakawa, A. Sasoh, K. Kojima, T. Kimura, Y. Kawamata, and M. Yasui, "Operation characteristics of applied-field magnetoplasmadynamics thruster using hollow cathode," *Transactions of the Japan Society for Aeronautical And Space Sciences, Aerospace Technology Japan,* vol. 16, no. 1 (2018), pp. 69-74.
4. D. Ichihara, T. Uno, H. Kataoka, J. Jeong, A. Iwakawa, and A. Sasoh, "Ten-ampere-level, applied-field-dominant operation in magnetoplasmadynamic thrusters," *Journal of Propulsion and Power,* vol. 33, no. 2 (2017), pp. 360-369.
5. J. Glowacki, R. A. Badcock, and N. Long, "Design analysis of a plasma thruster with superconducting magnets," in *AIAA Propulsion and Energy 2019 Forum* (2019), p. 4081.
6. M. Nisenoff and W. J. Meyers, "On-orbit status of the High Temperature superconductivity Space Experiment," *IEEE transactions on applied superconductivity,* vol. 11, no. 1 (2001), pp. 799-805.
7. A. Poghosyan and A. Golkar, "CubeSat evolution: Analyzing CubeSat capabilities for conducting science missions," *Progress in Aerospace Sciences,* vol. 88 (2017), pp. 59-83.
8. J. Olatunji, C. Acheson, M. Szmigiel, S. Wimbush, and N. Long, "Orbital and thermal modelling of a 3U CubeSat equipped with a high-temperature superconducting coil," *Acta Astronautica,* vol. 190 (2022), pp. 413-429.
9. R. Unger and D. Keiter, "The development of the CryoTel™ family of coolers," in *AIP Conference Proceedings*, American Institute of Physics, vol. 710, no. 1 (2004), pp. 1404-1411.
10. B. Leuw, J. Geng, J. H. Rice, D. A. Moseley, and R. A. Badcock, "A half-wave superconducting transformer-rectifier flux pump using J c (B) switches," *Superconductor Science and Technology,* vol. 35, no. 3 (2022), p. 035009.
11. J. Ekin, *Experimental techniques for low-temperature measurements: cryostat design, material properties and superconductor critical-current testing*, Oxford University Press (2006).